Journal of Alloys and Compounds 923 (2022) 166329

Contents lists available at ScienceDirect

Journal of Alloys and Compounds

journal homepage: www.elsevier.com/locate/jalcom

Research Article

Porous fluorine-doped tin oxide-anchored vanadium oxide films for multi-functional highly capacitive electrochromic layers

Seock-Joon Jeong[a,1], Kue-Ho Kim[a,1], Shuo Bai[b], Hyo-Jin Ahn[a,*]

[a] Department of Materials Science and Engineering, Seoul National University of Science and Technology, Seoul 01811, the Republic of Korea
[b] State Key Laboratory of Biochemical Engineering, Institute of Process Engineering, Chinese Academy of Sciences, 100190, Beijing, China

ARTICLE INFO

Article history:
Received 20 April 2022
Received in revised form 23 June 2022
Accepted 14 July 2022
Available online 16 July 2022

Keywords:
Films
Transition metal oxides
Pore structure
Multi-functional devices
Electrochromic energy storage performances

ABSTRACT

Electrochromic (EC) devices have been studied in recent decades as devices for optical property changes and energy-saving technologies, which has broadened their applications to include smart windows, sunglasses, and rear-view mirrors. Recently, multifunctional EC energy storage devices have attracted global attention because they can store and release energy during color changes. Herein, we demonstrate a hybrid composite structure of porous fluorine-doped tin oxide (FTO) microspheres on vanadium oxide films. Porous FTO microspheres were successfully synthesized using solvent-assisted ultrasonic spray pyrolysis. Vanadium oxide precursor solutions for the spin-coating process were prepared with porous FTO microsphere contents of 0, 1, 2, and 3 wt%. The hybrid composite EC energy storage film with 2 wt% porous FTO (V_2O_5-FTO2) exhibited superior EC and energy storage performances of widened transmittance modulation (53.79 % at 415 nm) and competitive specific capacitance (486.3 F/g at a high current density of 10 A/g) with high cyclic stability of 87.96 % up to 500 cycles. Thus, the suggested V_2O_5-FTO hybrid structure demonstrates feasibility as a promising research strategy for developing multifunctional highly capacitive electrochromic layers.

1. Introduction

Given the rapid increase in global energy consumption, the development of efficient energy storage media and energy saving technology have attracted huge global attention to prevent a further energy crisis [1]. Electrochemical devices such as lithium-ion batteries (LIBs), supercapacitors, and electrochromic (EC) devices have emerged as powerful alternatives to conventional fossil fuel-based energy sources because they provide significant advantages such as eco-friendliness, abundant source materials, and high efficiency [2–4]. In particular, EC systems have been introduced as a promising energy-saving strategy that can selectively adjust the sunlight penetration ratio by changing the transmittance [5–7]. General EC devices comprise three classes of functional layers: (1) EC layers for inducing redox reactions and color changes, (2) transparent conductive layers for electrical connections, and (3) electrolyte layers. To improve the performance of EC devices, it is important to modify the EC layers, which can directly affect the major characteristics of EC devices, such as the transmittance modulation, switching speeds, and coloration efficiency (CE) [8–10]. Metal oxide-based materials, such as V_2O_5, NiO, and WO_3 have been frequently adopted as EC layers owing to their high film transmittance, excellent electrochemical stability, and low cost [11–13]. In particular, vanadium oxide can provide high transmittance modulation and competitive energy storage performance, thereby expanding the application fields of EC layers [14]. Multifunctional capacitive EC layers can offer unique characteristics that simultaneously reflect the charging state of devices through color variations [15]. However, it is still difficult to achieve both a high specific capacity and high EC performance in multifunctional devices. To overcome this limitation, EC layers with high electrical conductivity, high transmittance, and good energy storage performance are required, which have not yet been broadly studied.

Fluorine-doped tin oxide (FTO) has attracted significant interest as a transparent conducting layer for optoelectrical devices owing to its high transmittance, high conductivity, and good chemical durability [16]. In addition, tin oxide (SnO_2) has been widely utilized as an anode material for LIBs because of its high Li-ion storage capability, with a theoretical capacity of ~782 mAh/g. The superior energy storage performance of FTO can be further enhanced by

* Corresponding author.
E-mail address: hjahn@seoultech.ac.kr (H.-J. Ahn).
[1] S.-J. Jeong and K.-H. Kim contributed equally to this work.

https://doi.org/10.1016/j.jallcom.2022.166329
0925-8388/

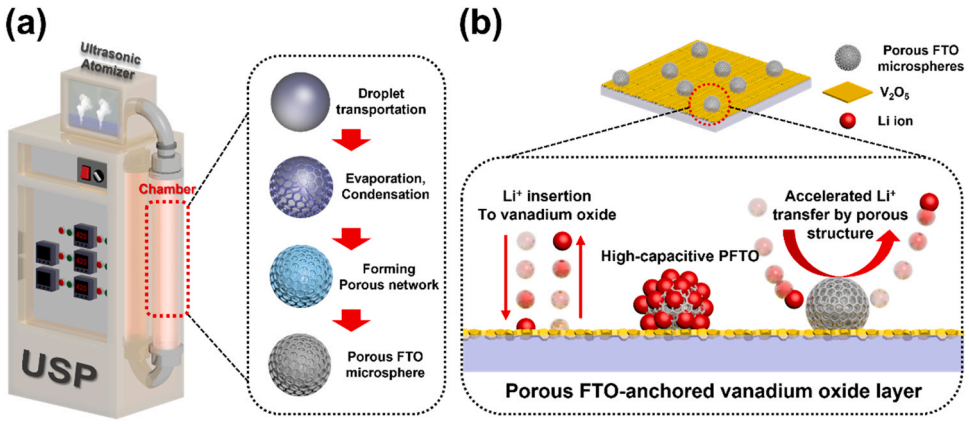

Fig. 1. (a) Schematic illustration of the synthetic route for the porous FTO microsphere by the ultrasonic spray pyrolysis and (b) advantages of the porous FTO microspheres anchored vanadium oxide layer for the electrochemical reactions.

generating pores, which effectively enlarge the specific surface area and offer favorable Li-ion diffusion pathways. Owing to these advantages, porous FTO is considered a promising active material for various electrochemical devices. However, the optical properties of FTO are difficult to control during the Li-ion insertion and desertion reactions, which limits the independent application of FTO for EC electrodes. Therefore, to develop a high-performance EC energy storage electrode, a hybrid composite structure of highly capacitive materials with an optically adjustable EC layer is required.

In this study, we report a porous FTO microsphere-anchored vanadium oxide film hybrid composite structure (V_2O_5-FTO) fabricated via ultrasonic spray pyrolysis (USP) followed by a sol-gel process. The porous FTO microspheres are homogeneously distributed on the vanadium oxide film in the optimized sample, and we demonstrate the effects of the components. Vanadium oxide offers an optically adjustable EC layer matrix, and porous FTO microspheres support the EC energy storage performance metrics, such as the specific capacity, switching speeds, and CE owing to their highly capacitive characteristics and high electrical conductivity. Thus, the fabricated V_2O_5-FTO electrode exhibits excellent EC energy storage performance, and its applicability as a multifunctional device is evaluated using a full cell with a Pt electrode.

2. Experimental details

The capacitive EC layer was prepared via a spin-coating process using a mixture of porous FTO microspheres and V_2O_5 precursor solution. The porous FTO powder was synthesized using USP with a vertical chamber. To synthesize the porous FTO microspheres, a precursor solution was first prepared by dissolving 0.68 M tin chloride pentahydrate ($SnCl_4.5\ H_2O$, SAMCHUN) and 1.2 M ammonium fluoride (NH_4F, JUNSEI) in deionized (DI) water. After vigorous stirring for 3 h, 50 vol% organic solvent (acetone, SAMCHUN) was added to the precursor solution for the solvent-assisted USP process. After vigorous stirring for 3 h, the transparent solution was poured into an ultrasonic atomizer (1.6 MHz). In order to generate the droplet, we applied DC 40 V to the ultrasonic atomizer and the generated droplets were carried into the vertical chamber. The pyrolysis temperature of the vertical chamber was fixed at 420 °C using the upper, middle, and lower heaters. The flow rate of the carrier gas (air consisting of 21 % O_2 with a balance of N_2) was set to 2.5 L/min. The resultant powder was collected through a stainless mesh bag filter (stainless steel, SUS 304), and porous FTO microspheres were obtained by sweeping off the filter. To synthesize the sol precursor for the solvothermal method, 0.4 g of vanadium chloride (VCl_3, Alfa Aesar) was dissolved in ethanol (CH_3CH_2OH, Aldrich). Then, the sol precursor was poured into an autoclave for a 10 h solvothermal process at 180 °C. After centrifugation, the resultant vanadium precipitates were dissolved in 2-propanol ($(CH_3)_2CHOH$, Aldrich) to prepare the precursor solution for the spin-coating process. Then, the porous FTO powder was added in varying amounts of 0, 1, 2, and 3 wt% (hereafter referred to as bare V_2O_5, V_2O_5-FTO1, V_2O_5-FTO2 and V_2O_5-FTO3, respectively). To prepare the EC electrode, the spin-coating process was conducted with the resultant precursor solutions on commercial FTO substrates (2000 rpm for 30 s) and then heat-treated to 450 °C in a box furnace. The mass of coated active material was fixed at ~20 μg/cm^2 for all the fabricated films to obtain the reliable results.

The morphologies of the prepared films were observed using field-emission scanning electron microscopy (FESEM: Hitachi, S-4800). X-ray diffraction (XRD: Bruker DE/D8 Advance using Cu Kα radiation) was performed to identify the crystal structure, and the chemical states were characterized using X-ray photoelectron spectroscopy (XPS: ESCALAB 250, Al Kα source). To measure the electrical properties, a Hall effect measurement system (Ecopia, HMS-3000) was utilized. The electrochemical properties were estimated using a potentiostat/galvanostat (PGSTAT302 N, FRA32 M, Metrohm Autolab B.V., Netherlands) comprising a three-electrode system with Ag wire as the reference electrode and Pt wire as the counter electrode in 1 M $LiClO_4$ (dissolved in propylene carbonate) electrolyte. Transmittance variations at a wavelength of 415 nm were recorded using ultraviolet-visible (UV–vis) spectroscopy (Perkin-Elmer, Lambda-35) during the electrochemical measurements.

3. Results and discussion

Porous FTO-anchored vanadium oxide films were prepared via a two-step procedure using USP followed by spin-coating process. Fig. 1a shows the synthesis procedure for the porous FTO microspheres. Highly porous microspheres were successfully obtained using an organic solvent-assisted USP process. The precursor solution was prepared from a mixed solvent of DI water and a highly volatile organic solvent (acetone), which had different boiling points (BP) (100 °C for DI water and 56 °C for acetone). Interestingly, the difference in the BPs of the solvents induced a unique phenomenon during the USP process, generating a highly porous particle morphology [17]. The USP process can be divided into four steps: (1) atomization of the precursor solution, (2) droplet transportation, (3) solvent evaporation, and (4) crystallization. In the first step, the ultrasonic atomizer generates micro-scale precursor droplets, the amount and sizes of which can be adjusted by changing the manufacturing parameters, such as the frequency, amplitude, and time. Second, the generated droplets are transported to the pyrolysis chamber along with the gas flow. Third, the solvent in the

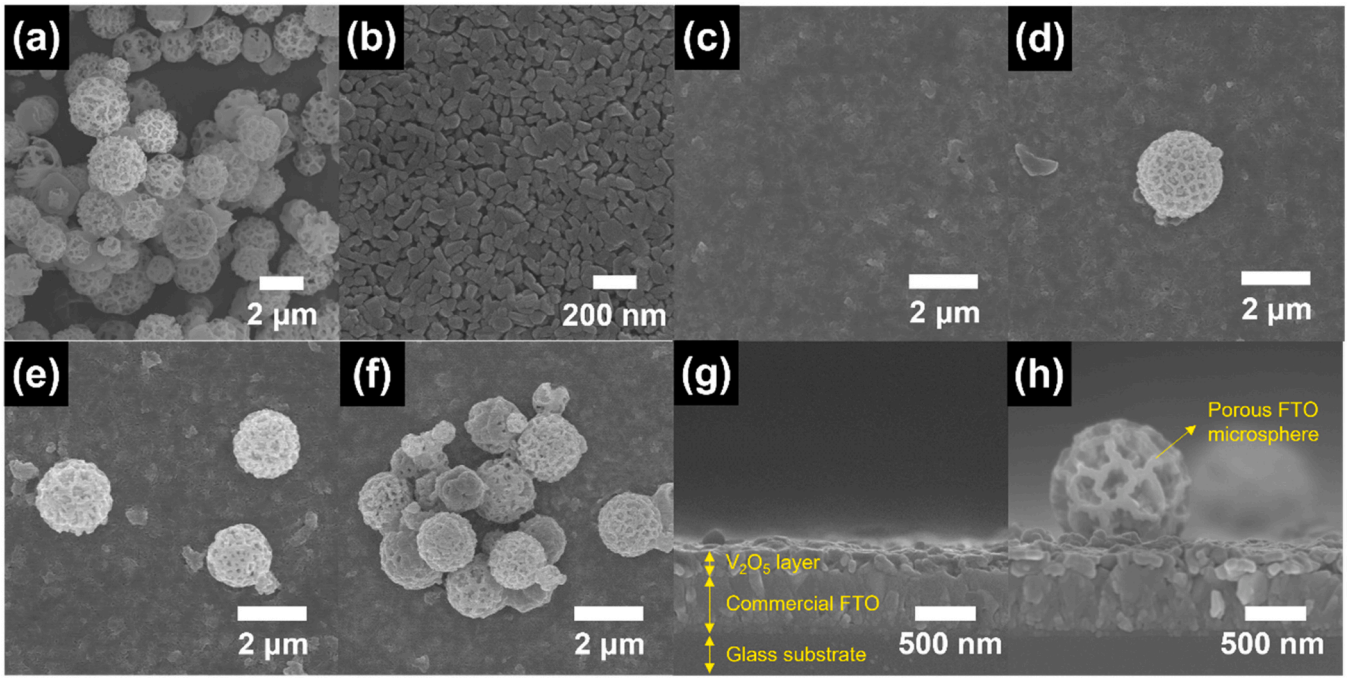

Fig. 2. FESEM image of (a) FTO microspheres, top-view images of (b,c) bare V_2O_5, (d) V_2O_5-FTO1, (e) V_2O_5-FTO2, (f) V_2O_5-FTO3, cross-view images of (g) bare V_2O_5, and (h) V_2O_5-FTO2.

transported droplets evaporates due to the heat of the pyrolysis chamber, and the droplets gradually transform to precipitated particles. During this step, the acetone solvent evaporates earlier than the DI water because of its lower boiling point, which generates a pore structure in the FTO microspheres. Finally, the precipitated particles become solid particles with the decomposition of the precursor in the pyrolysis chamber. To prepare the highly capacitive EC layer, various amounts (1 wt%, 2 wt%, and 3 wt%) of porous FTO microspheres were dispersed in a vanadium oxide precursor solution and coated onto commercial FTO glass using a spin-coating method. In Fig. 1b, the resultant porous FTO-anchored vanadium oxide layers were successfully fabricated and the optimized film morphology could boost the performance of capacitive EC layer. During the electrochemical reactions, Li^+ can be inserted into both the vanadium oxide film and porous FTO microspheres, enabling a large energy storage capability with a simultaneous transmittance change [18]. Moreover, the porous structure of the FTO microspheres offers a favorable Li^+ transfer pathway with high electrical conductivity, which can facilitate the energy storage performance at high current densities and reduce the switching speed [19].

Fig. 2 presents FESEM images of the fabricated samples to confirm the surface morphology. In Fig. 2a, the FTO microspheres show predominantly highly porous structures with size of 1.89–2.76 μm (2.24 μm on average). Interestingly, the FTO microspheres show randomly developed porous morphologies owing to the synthesis mechanism during the USP process. The morphology can be varied according to the arrangement of the organic solvent within the precursor droplets, which results in this morphological characteristic. Fig. 2b shows a high-resolution FESEM image of the bare V_2O_5 film, revealing a particle size range of ~91.7 nm to ~149.3 nm. This homogeneous rod-like film morphology is a typical structure of vanadium oxide with a relatively low sintering temperature (450 °C). To investigate the morphology of the V_2O_5-FTO hybrid composite structure, low-resolution FESEM images were obtained for bare V_2O_5, V_2O_5-FTO1, V_2O_5-FTO2, and V_2O_5-FTO3 (Fig. 2c–f, respectively). As expected, bare V_2O_5 exhibits a uniform and smooth film morphology without any composite materials. In addition, the amount of anchored porous FTO microspheres increases as the amount of added porous FTO increases from 1 wt% to 3 wt%. Among them, the V_2O_5-FTO2 film appears to be the optimized hybrid composite structure with well-distributed porous FTO microspheres on the vanadium oxide film. When the amount of porous FTO added reaches 3 wt%, the microspheres agglomerate because of the excessive amount of porous FTO. This agglomeration reduces the porous FTO dispersion level on the vanadium oxide film, degrading the hybrid composite effects, such as the electrical conductivity enhancement [20,21]. To confirm the thickness of the vanadium oxide films and the detailed composite structure, cross-view FESEM images were also obtained for the bare V_2O_5 and V_2O_5-FTO2 electrodes (Fig. 2g and h, respectively). Both V_2O_5 layers show a uniform thickness of 176.4–181.5 nm, and V_2O_5-FTO2 shows anchored porous FTO microspheres on the vanadium oxide film. A porous FTO-anchored film morphology is developed owing to the difference in V_2O_5 film thickness and the size of porous FTO microspheres, exposing a large surface area of porous FTO, which can improve the the improved energy storage performance with sufficient Li^+ insertion sites [22,23]. In addition, to investigate interior structure in detail, we conducted TEM analysis of porous FTO microspheres, bare V_2O_5, and V_2O_5-FTO2 (Fig. S1). In Fig. S1a, the difference between light and dark regions were confirmed, signifying the overall porous structure of porous FTO microspheres. Fig. S1b,c shows the morphology of the bare V_2O_5, and V_2O_5-FTO2, which results are well-matched with the FESEM data.

Fig. 3a shows the XRD results obtained for the bare V_2O_5, V_2O_5-FTO1, V_2O_5-FTO2, and V_2O_5-FTO3 samples. The two peaks observed at approximately around 20.2° and 26.1° correspond to the orthorhombic (001) and (110) crystal structures of V_2O_5, respectively. Owing to the low amount of added porous FTO, there is no distinguishable change between the bare V_2O_5 and the other samples. The Raman analysis was also conducted after being coating on bare glass substrates (Fig. S2). According to the results, all samples showed bonding and stretching modes of V_2O_5 orthorhombic phase, and the peaks of FTO were overlapped by V_2O_5 peaks at ~148 cm^{-1} and 475 cm^{-1} due to the similar peak location with low amount of porous FTO microspheres. The peaks were indicated by blue letters and can be assigned with a stoichiometric SnO_x phase ($1 < x < 2$) and band

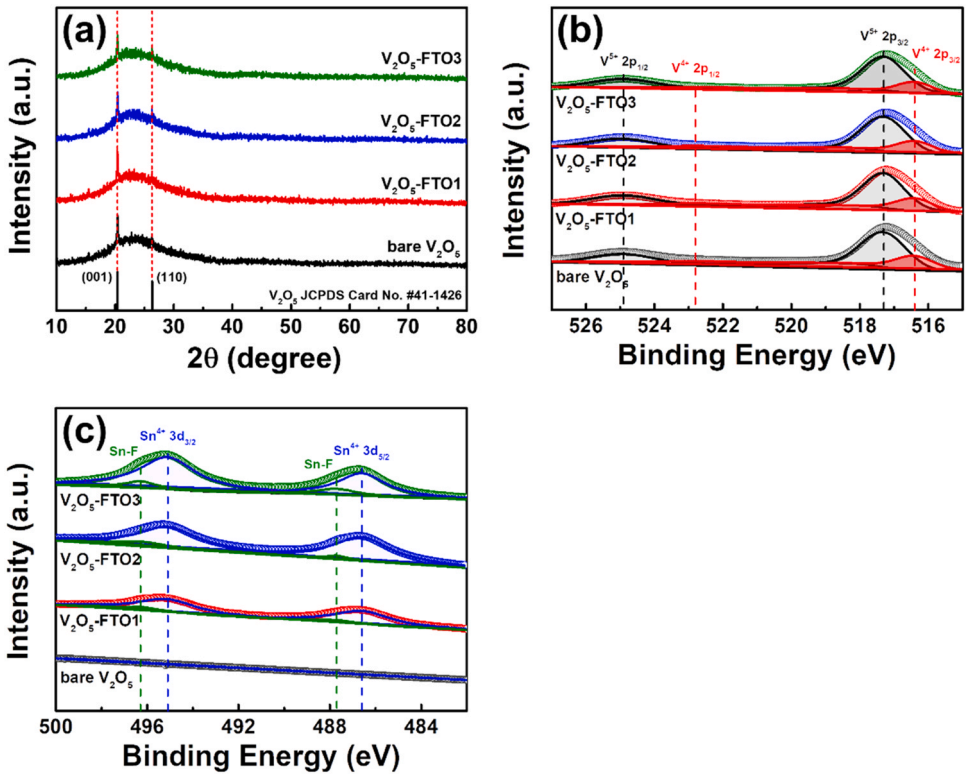

Fig. 3. (a) XRD curves and XPS core-level spectra of (b) V 2p, (c) Sn 3d obtained from bare V_2O_5, V_2O_5-FTO1, V_2O_5-FTO2, and V_2O_5-FTO3.

gap energy for SnO_2, respectively. Moreover, XPS analysis was performed to determine the detailed structural properties. Fig. 3b shows the XPS results for the V 2p region, exhibiting four peaks at around 524.9, 522.8, 517.3, and 516.4 eV, corresponding to V^{5+} $2p_{1/2}$, V^{4+} $2p_{1/2}$, V^{5+} $2p_{3/2}$, and V^{4+} $2p_{3/2}$, respectively. Fig. 3c shows the Sn 3d core-level spectra, demonstrating the existence of porous FTO microspheres in the V_2O_5-FTO1, V_2O_5-FTO2, and V_2O_5-FTO3 films compared to the bare V_2O_5 film with no peak. The films with porous FTO added show Sn-F bonding at around 496.3 eV and 487.7 eV, which confirms that the F-doped tin oxide structure was developed successfully. Further, Sn^{4+} $3d_{3/2}$ and Sn^{4+} $3d_{5/2}$ bonds are observed at around 495.1 eV and 486.6 eV, respectively [24,25]. Thus, the successful formation of the orthorhombic V_2O_5 structure and the hybrid composite structure with porous FTO microspheres are confirmed by these results.

Fig. 4a shows the electrical conductivities of the films, which can directly affect the EC energy storage performance. The films were prepared on an insulating bare glass substrate to obtain precise electrical properties using a Hall effect measurement system. As the amount of porous FTO increases, the electrical conductivity improves. Here, the V_2O_5-FTO2 shows the highest electrical conductivity of 5.01×10^{-5} S/cm among all the samples (compared to 3.47×10^{-5}, 4.69×10^{-5}, and 4.36×10^{-5} S/cm for bare V_2O_5, V_2O_5-FTO1, and V_2O_5-FTO3, respectively). The excellent electrical characteristics are attributed to the well-dispersed porous FTO microspheres, which possess high electrical conductivity. Interestingly, V_2O_5-FTO3 shows lower electrical conductivity than V_2O_5-FTO2 because of the excessive addition of porous FTO, which induce agglomeration. The electrochemical impedance spectroscopy (EIS) data for all the electrodes are shown in Fig. 4b with the applied circuit model. The EIS data generally comprise R_s (composite resistance of the electrode), R_{ct} (charge transfer resistance), Z_w (Warburg resistance), C_{dl} (double-layer capacitance), and C_{ps} (pseudocapacitance), which circuit model is depicted in Fig. S3. The Nyquist plots present a single semicircle in the high-frequency region and an inclined line in the low-frequency region. The semicircle commonly projects the internal resistance of the electrode, and the slope signifies the ion diffusivity. V_2O_5-FTO2 exhibits the smallest semicircle,

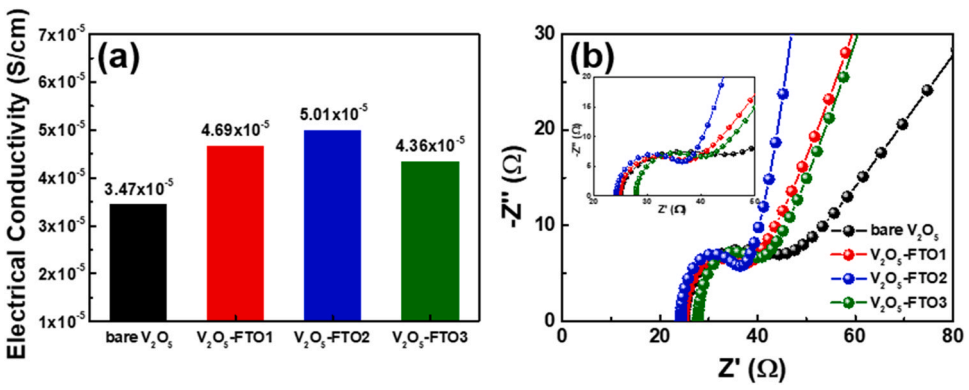

Fig. 4. (a) Electrical conductivity and (b) Nyquist plots of EIS results obtained from bare V_2O_5, V_2O_5-FTO1, V_2O_5-FTO2, and V_2O_5-FTO3.

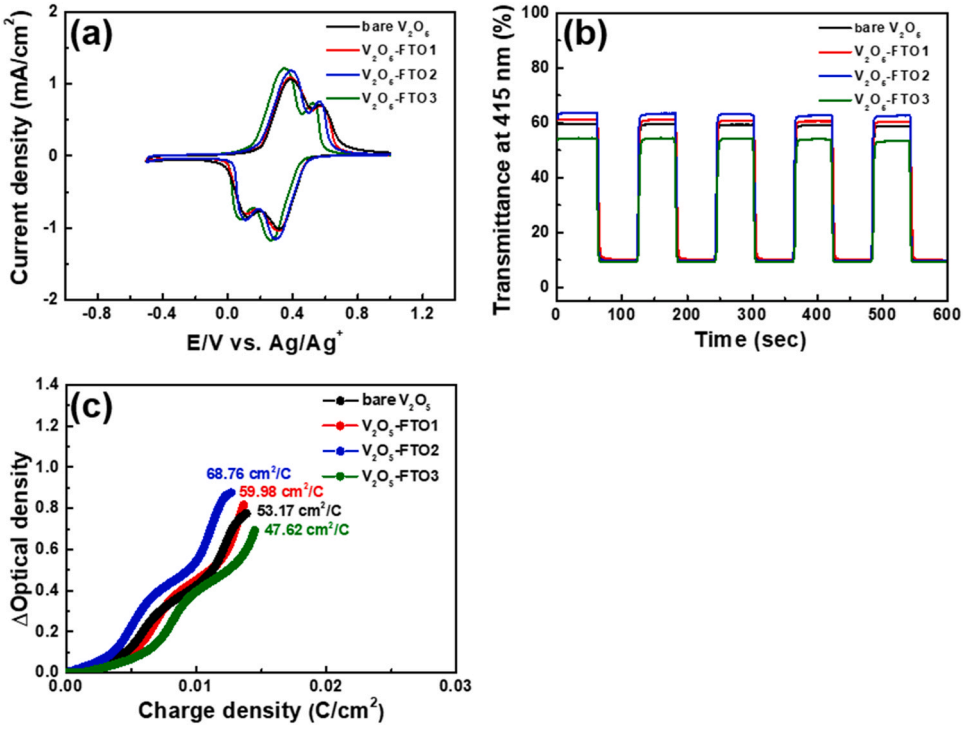

Fig. 5. (a) CV curves measured between −0.5 V and 1.0 V at a scan rate of 20 mV/s, (b) *In-situ* optical transmittance curves chased at a stepping potential of −0.5 V and 1.0 V for 60 s per process, and (c) optical density variations at 415 nm induced by inserted charge density.

implying high electrical conductivity. In addition, the V_2O_5-FTO2 sample shows the steepest slope in the low-frequency zone. These results are caused by the hybrid composite structure of well-dispersed porous FTO, which provides high electrical conductivity with additional Li^+ storage sites and favorable ion transfer pathways [26].

Cyclic voltammetry (CV) analyses were performed to determine the electrochemical characteristics. Each of the CV curves in Fig. 5a was obtained in 1 M $LiClO_4$ electrolyte from − 0.5–1.0 V with a fixed potential rate of 20 mV/s. In this potential range, the electrochemical reaction can be represented by the following equation [27,28]:

$$V_2O_5\ (\text{colored}) + x\ Li^+ + x\ e^- \leftrightarrow Li_xV_2O_5\ (\text{bleached}) \quad (1)$$

Here, −0.5 V promotes the intercalation of Li^+ into the V_2O_5 structure, which forms $Li_xV_2O_5$ in a bleached state. When the opposite potential of + 1.0 V is applied, Li^+ is released from the $Li_xV_2O_5$ lattices to form V_2O_5 again, which is a stable phase at the anodic potential. As the amount of porous FTO increases, the CV peak area increased, signifying enhanced capacitance of the electrochemical reactions [29]. The shifted CV peaks to lower values for the porous FTO composite samples are attributed to the low Li^+ insertion voltage of porous FTO compared with that of the V_2O_5 matrix [30]. To evaluate the EC performance, the transmittance variations were traced with chronoamperometry analysis using applied potentials of − 0.5 V and 1.0 V at a wavelength of 415 nm (Fig. 5b). Here, ΔT is defined as the difference between the highest transmittance at the bleached state (T_b) and the lowest transmittance in the colored state (T_c). Furthermore, the switching speeds are defined as the time required to reach 90 % transmittance of the bleached and colored states. Notably, V_2O_5-FTO2 shows the fastest switching speeds (2.1 s to reach the colored state and 4.1 s for the bleached state) with the widest ΔT of 53.79 %, which is mainly caused by the optimized hybrid composite structure of V_2O_5 and porous FTO microspheres. V_2O_5-FTO3 exhibits a poor ΔT and switching speeds compared with V_2O_5-FTO2. The excessive amount of porous FTO microspheres degrades the hybrid composite effects due to the agglomerated porous FTO microspheres [31]. These results imply that the optimized addition amount and distribution of the porous FTO microspheres are the main factors affecting ΔT and the switching speeds. Furthermore, as a crucial factor for the EC performance, CE is calculated using Eq. (2) [32,33]:

$$CE = \triangle OD/(Q/A) \quad (2)$$

$$\triangle OD = \log\ (T_b/T_c) \quad (3)$$

where Q indicates the integrated charge, and A is the reaction area. Fig. 5c shows the curves of the optical density (OD) variation according to the applied charge density at 415 nm. The CE values are calculated as 53.17, 59.98, 68.76, and 47.62 cm^2/C for the bare V_2O_5, V_2O_5-FTO1, V_2O_5-FTO2, and V_2O_5-FTO3 samples, respectively. The greatest CE value is obtained for V_2O_5-FTO2, and this result can be attributed to the successfully composed hybrid composite structure of V_2O_5 and porous FTO microspheres. To confirm the energy storage performance and verify the potential for multifunctional EC energy storage applications, Fig. 6 shows the specific capacitances (C_{sp}) of the bare V_2O_5 and V_2O_5-FTO2 films with varied current densities of 2, 4, 6, 8, and 10 A/g. The specific capacitances were calculated using discharge time of galvanic charge-discharge curves (Fig. S4) according to Eq. (4) below [34]:

$$C_{sp} = I/(mdV/dt) \quad (4)$$

At these current densities, the specific capacitances of V_2O_5-FTO2 are 532.9, 513.9, 504.6, 492.3, and 486.3 F/g, respectively. Moreover, the cyclic stability of bare V_2O_5 and V_2O_5-FTO2 was also evaluated by applying − 0.5 V and 1.0 V sequentially for 500 cycles (Fig. S5). V_2O_5-FTO2 exhibits superior retention of transmittance modulation from 54.83 % to 48.23 % after 500 cycles (retention rate of 87.96 %) compared with the bare V_2O_5 film (retention rate of 82.01 %). This result demonstrates the high cyclic stability of V_2O_5-FTO2 due to the improved electrical conductivity by porous

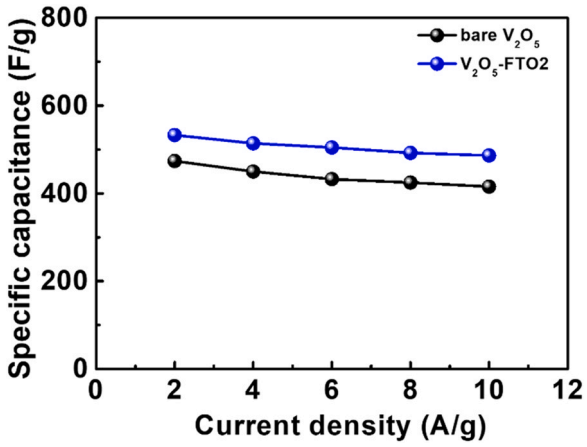

Fig. 6. (a) Specific capacitances of bare V_2O_5 and V_2O_5-FTO2 with varied current densities of 2, 4, 6, 8, and 10 A/g.

FTO microspheres. In Fig. S6, SEM analysis after 500 cycles of bare V_2O_5 and V_2O_5-FTO2 was also performed to investigate the degree of morphology change. After 500 cycles, both samples appeared the agglomeration of V_2O_5 particles by repeated cycles. However, the porous FTO microspheres maintain their initial morphology, which has a significant impact on the cyclic stability of the V_2O_5-FTO2. To investigate the full cell energy storage performances, galvanostatic charge-discharge curves of bare V_2O_5 and V_2O_5-FTO2 full cell were measured with varied current densities of 2.0, 4.0, 6.0, 8.0, and 10.0 A/g in Fig. S7a,b. Also, we added the specific capacitance retention and coulombic efficiency at a current density of 2.0 A/g during 10 cycles in Fig. S7c. Both bare V2O5 and V2O5-FTO2 full cell show angled galvanostatic charge-discharge curves, implying the pseudocapacitive reactions. Moreover, V2O5-FTO2 full cell exhibited excellent specific capacitance and cycle stability compared with bare V2O5, maintaining high coulombic efficiency. This result is mainly contributed to the high-capacitive porous FTO microspheres, which possess large active area with high electrical conductivity. This competitive energy storage performance is attributed to the well-dispersed porous FTO microspheres, which offer additional Li^+ storage sites with favorable ion transfer pathways.

To demonstrate the practical application of porous FTO-anchored vanadium oxide films as multifunctional EC energy devices, 4 cm × 4 cm EC devices were fabricated using bare V_2O_5 and V_2O_5-FTO2 as working electrodes and Pt-coated glass as the counter-electrode with a 2.5 M $LiClO_4$ gel polymer electrolyte. Fig. 7a shows photographs of the colored (2.5 V, discharged) and bleached (−2.5 V, charged) states of the fabricated EC devices with the V_2O_5-FTO2 electrode, which confirm the color change based on the charging state. To compare the energy storage capability of the EC devices, LEDs were operated using charged EC devices (Fig. 7b). The lighting times of the EC devices are measured as ~17 s for bare V_2O_5 and ~24 s for V_2O_5-FTO2, which is consistent matches with the specific capacitance data in Fig. 6. Thus, the EC devices with the V_2O_5-FTO2 working electrode exhibit competitive energy storage performance along with optimized EC performance.

In this study, we developed highly capacitive porous FTO-anchored vanadium oxide layers and confirmed the feasibility of their application in multifunctional EC energy storage devices. The V_2O_5-FTO2 film showed optimized EC performance including high transmittance modulation, fast switching speeds, and a high CE value, which are attributed to the high electrical conductivity and large bandgap of the composite porous FTO microspheres. Moreover, the V_2O_5-FTO2 film exhibited a superior specific capacity owing to the additional Li^+ storage sites of porous FTO with favorable ion transfer pathways. Thus, porous FTO-anchored vanadium oxide layers with optimized EC energy storage performance can be utilized as competitive candidates for multifunctional EC energy storage devices. Table 1.

Table 1
Summary of EC performances measured from all V_2O_5 electrodes.

Samples	T_b (%)	T_c (%)	Transmittance modulation (%, 415 nm)	Coloration speed (s)	Bleaching speed (s)	CE (cm^2/C)
bare V_2O_5	59.53	9.51	50.02	4.8	5.3	53.17
V_2O_5-FTO1	61.19	10.04	51.15	3.9	5.7	59.98
V_2O_5-FTO2	63.8	10.01	53.79	2.1	4.1	68.76
V_2O_5-FTO3	54.42	9.19	45.23	3.9	7.6	47.62

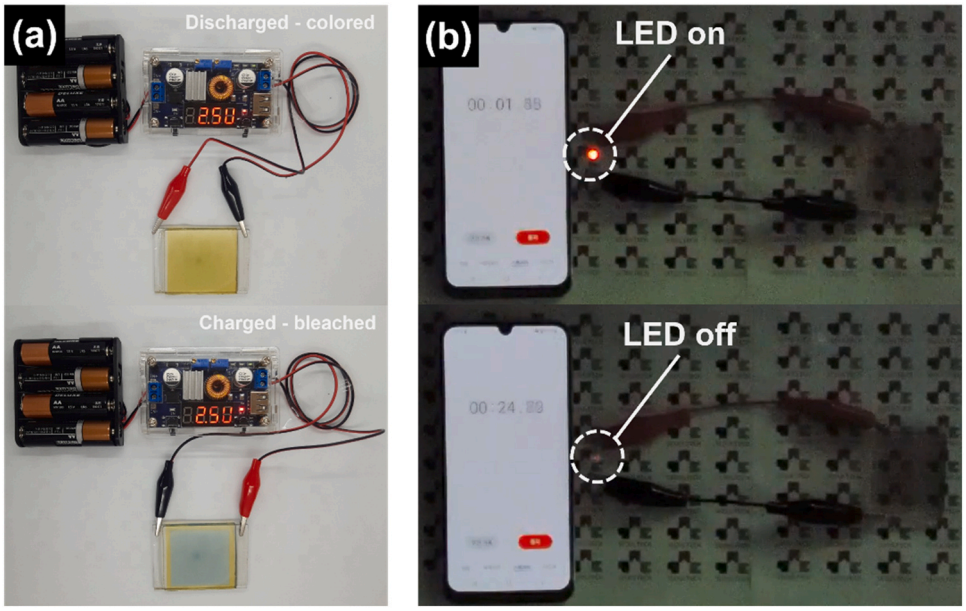

Fig. 7. (a) Photograph of operated electrochromic energy-storage multi-functional device at ± 2.5 V and (b) time-driven images of lighting LEDs during discharging process.

4. Conclusion

In this study, we developed porous FTO-anchored vanadium oxide films for multifunctional EC energy storage device applications. Highly porous FTO microspheres were successfully synthesized using a solvent-assisted USP process. Moreover, by adjusting the amount of porous FTO added, a hybrid composite structure of vanadium oxide with well-dispersed porous FTO microspheres was obtained. The optimized V_2O_5-FTO2 exhibited good EC performance, such as rapid switching speeds (2.1 s and 4.1 s for coloration and bleaching, respectively), a high transmittance modulation of 53.79 %, and the highest CE value of 68.76 cm^2/C. Moreover, V_2O_5-FTO2 also showed a competitive specific capacitance of 486.3 F/g at a high current density of 10 A/g. The EC performance enhancements were attributed to the composite porous FTO microspheres, which possessed high electrical conductivity with a large bandgap, leading to fast switching speeds and high transmittance modulation. Moreover, the porous FTO microspheres provided additional Li^+ storage sites with favorable ion transfer pathways, which improved the specific capacitance. Therefore, V_2O_5-FTO2 is a promising candidate for multifunctional EC energy storage devices.

CRediT authorship contribution statement

Seock-Joon Jeong: Conceptualization, Methodology, Writing – original draft. **Kue-Ho Kim:** Methodology, Investigation. **Shuo Bai:** Investigation. **Hyo-Jin Ahn:** Conceptualization, Supervision. Writing – review & editing.

Data availability

Data will be made available on request.

Declaration of Competing Interest

The authors declare that they have no known competing financial interests or personal relationships that could have appeared to influence the work reported in this paper.

Acknowledgements

This study was supported by the Research Program funded by the SeoulTech (Seoul National University of Science and Technology).

Appendix A. Supporting information

Supplementary data associated with this article can be found in the online version at doi:10.1016/j.jallcom.2022.166329.

References

[1] J.B. Goodenough, Y. Kim, Challenges for rechargeable Li batteries, Chem. Mater. 22 (2010) 587–603.
[2] M. Qian, Y. Tang, L. Liu, Y. Gao, X. Li, Well-dispersed $Li_2CoTi_3O_8$ nanoparticles as a multifunctional material for lithium-ion batteries and lithium-sulfur batteries, J. Alloy. Compd. 896 (2022) 162926.
[3] P. Forouzandeh, P. Ganguly, R. Dahiya, S.C. Pillai, Supercapacitor electrode fabrication through chemical and physical routes, J. Power Sources 519 (2022) 230744.
[4] K.-H. Kim, S.-J. Jeong, B.-R. Koo, H.-J. Ahn, Surface amending effect of N-doped carbon-embedded NiO films for multirole electrochromic energy-storage devices, Appl. Surf. Sci. 537 (2021) 147902.
[5] S.Y. Kim, Y.J. Jang, Y.M. Kim, J.K. Lee, H.C. Moon, Tailoring diffusion dynamics in energy storage ionic conductors for high-performance, multi-function, single-layer electrochromic supercapacitors, Adv. Funct. Mater. (2022) 2200757.
[6] M.-H. Jo, B.-R. Koo, K.-H. Kim, H.-J. Ahn, Tailored interface stabilization of FTO transparent conducting electrodes boosting electron and Li ion transport for electrochromic energy-storage devices, Chem. Eng. J. 431 (2022) 134036.
[7] W. Liu, X. Zhang, J. Liu, X. Ma, J. Zeng, P. Liu, T. Xu, Electrochromic properties of organic-inorganic composite materials, J. Alloy. Compd. 718 (2017) 379–385.
[8] D. Ma, G. Shi, H. Wang, Q. Zhang, Y. Li, Hierarchical NiO microflake films with high coloration efficiency, cyclic stability and low power consumption for applications in a complementary electrochromic device, Nanoscale 5 (2013) 4808.
[9] H. Ling, J. Wu, F. Su, Y. Tian, Y.J. Liu, Automatic light-adjusting electrochromic device powered by perovskite solar cell, Nat. Commun. 12 (2021) 1010.
[10] B.-R. Koo, K.-H. Kim, H.-J. Ahn, Novel tunneled phosphorus-doped WO_3 films achieved using ignited red phosphorus for stable and fast switching electrochromic performances, Nanoscale 11 (2019) 3318–3325.
[11] Y. Wang, G. Shen, T. Tang, J. Zeng, R.U.R. Sagar, X. Qi, T. Liang, Construction of doped-rare earth (Ce, Eu, Sm, Gd) WO3 porous nanofilm for superior electrochromic and energy storage windows, Electrochim. Acta 412 (2022) 140099.
[12] P. Liu, S.-H. Lee, C.E. Tracy, J.A. Turner, J.R. Pitts, S.K. Deb, Electrochromic and chemochromic performance of mesoporous thin-film vanadium oxide, Solid State Ion. 165 (2003) 223–228.
[13] X. Zhan, F. Gao, Q. Zhuang, Y. Zhang, J. Dang, Two-dimensional porous structure of V-doped NiO with enhanced electrochromic properties, ACS Omega 7 (2022) 8960–8967.
[14] S. Zhang, S. Chen, Y. Luo, B. Yan, Y. Gu, F. Yang, Y. Cao, Large-scale preparation of solution-processable one-dimensional V_2O_5 nanobelts with ultrahigh aspect ratio for bifunctional multicolor electrochromic and supercapacitor applications, J. Alloy. Compd. 842 (2020) 155882.
[15] H. Liu, X. Liang, T. Jiang, Y. Zhang, S. Liu, X. Wang, X. Fan, X. Huai, Y. Fu, Z. Geng, D. Zhang, Analysis of structural morphological changes from 3DOM V_2O_5 film to V_2O_5 nanorods film and its application in electrochromic device, Sol. Energy Mater. Sol. Cells 238 (2022) 111627.
[16] A. Korjenic, K.S. Raja, Electrochemical stability of fluorine doped tin oixde (FTO) coating at different Ph conditions, J. Electrochem. Soc. 166 (2019) C169–C184.
[17] M. Okuya, K. Shiozaki, N. Horikawa, T. Kosugi, G.R.A. Kumara, J. Madarász, S. Kaneko, G. Pokol, Porous TiO_2 thin films prepared by spray pyrolysis deposition (SPD) technique and their application to UV sensors, Solid State Ion. 172 (2004) 527–531.
[18] B.-R. Koo, K.-W. Sung, H.-J. Ahn, Boosting ultrafast lithium storage capability of hierarchical core/shell constructed carbon nanofiber/3D interconnected hybrid network with nanocarbon and FTO nanoparticle heterostructures, Adv. Funct. Mater. 30 (2020) 2001863.
[19] H.Z. Asl, S.M. Rozati, High-quality spray-deposited fluorine-doped tin oxide: effect of film thickness on structural, morphological, electrical, and optical properties, Appl. Phys. A Mater. Sci. Process. 125 (2019) 689.
[20] J. Sun, L. Xiao, S. Jiang, G. Li, Y. Huang, J. Geng, Fluorine-doped SnO_2@graphene porous composite for high capacity lithium-ion batteries, Chem. Mater. 27 (2015) 4594–4603.
[21] R.J. Cembrola, The relationship of carbon black dispersion to electrical resistivity and vulcanizate physical properties, Polym. Eng. Sci. 22 (1982) 601–609.
[22] Y. Pan, L. Li, S.H. Chan, J. Zhao, Correlation between dispersion state and electrical conductivity of MWCNTs/PP composites prepared by melt blending, Compos. Part A 41 (2010) 419–426.
[23] F. Xu, Z. Tang, S. Huang, L. Chen, Y. Liang, W. Mai, H. Zhong, R. Fu, D. Wu, Facile synthesis of ultrahigh-surface-area hollow carbon nanospheres for enhanced adsorption and energy storage, Nat. Commun. 6 (2015) 7221.
[24] J. Yang, J. Wang, D. Wang, X. Li, D. Geng, G. Liang, M. Gauthier, R. Li, X. Sun, 3D porous $LiFePO_4$/graphene hybrid cathodes with enhanced performance for Li-ion batteries, J. Power Sources 208 (2012) 340–344.
[25] S.-J. Jeong, K.-H. Kim, H.-J. Ahn, Vacancy-engineered V_2O_{5-x} films for ultrastable electrochromic applications, Ceram. Int. 48 (2022) 9400–9406.
[26] H. Song, C. Liu, C. Zhang, G. Cao, Self-doped V^{4+}-V_2O_5 nanoflake for 2 Li-ion intercalation with enhanced rate and cycling performance, Nano Energy 22 (2016) 1–10.
[27] K.-H. Kim, B.-R. Koo, H.-J. Ahn, Effects of Sb-doped SnO_2-WO_3 nanocomposite on electrochromic performance, Ceram. Int. 45 (2019) 15990–15995.
[28] G. Li, W. Lei, D. Luo, Y.-P. Deng, D. Wang, Z. Chen, 3D porous carbon sheets with multidirectional ion pathways for fast and durable lithium-sulfur batteries, Adv. Energy Mater. 8 (2018) 1702381.
[29] L. Shao, K. Wu, X. Lin, M. Shui, R. Ma, D. Wang, N. Long, Y. Ren, J. Shu, Sol-gel preparation of V_2O_5 sheets and their lithium storage behaviors studied by electrochemical and in-situ X-ray diffraction techniques, Ceram. Int. 40 (2014) 6115–6125.
[30] J. Shin, H. Jung, Y. Kim, J. Kim, Carbon-coated V_2O_5 nanoparticles with enhanced electrochemical performance as a cathode material for lithium ion batteries, J. Alloy. Compd. 589 (2014) 322–329.
[31] G. Kim, B.-H. Kim, One-dimensional hierarchical porous carbon nanofibers with cobalt oxide in a hollow channel for electrochemical applications, J. Alloy. Compd. 910 (2022) 164886.
[32] H. Krýsová, M.N. Spallart, H. Tarábková, P. Janda, L. Kavan, J. Krýsa, Atomic layer deposited films of Al_2O_3 on fluorine-doped tin oxide electrodes: stability and barrier properties, Beilstein J. Nanotechnol. 12 (2021) 24–34.
[33] M.-H. Jo, B.-R. Koo, H.-J. Ahn, Defective impacts on amorphous $WO_3 \cdot H_2O$ films using accelerated hydrolysis effects for flexible electrochromic energy-storage devices, Appl. Surf. Sci. 556 (2021) 149664.
[34] H. Wang, C.-J. Yao, H.-J. Nie, L. Yang, S. Mei, Q. Zhang, Recent progress in integrated functional electrochromic energy storage devices, J. Mater. Chem. C 8 (2020) 15507–15525.